

Population-Dominated Ergotropy in a Capacitively Coupled Double-Quantum-Dot Battery under $1/f$ Charge Noise

Khalil Loukhssami ^{1,*} Khadija El Hawary ^{1,†} Sanaa Abaach ¹ and Morad El Baz ¹

¹*ESMaR, Department of Physics, Faculty of Sciences,
Mohammed V University in Rabat, Rabat, Morocco*

(Dated: June 29, 2026)

We investigate extractable work storage in a capacitively coupled double quantum dot (DQD) quantum battery (QB) subjected to experimentally motivated detuning charge noise. The battery is modeled as two interacting charge qubits with an Ising-type capacitive coupling and is charged by resonant microwave modulation of the tunnel coupling channel. Detuning fluctuations are introduced as classical stochastic processes generated from a band limited $1/f$ noise spectrum. For each noise realization, the evolution remains unitary, whereas decoherence and loss of contrast emerge after ensemble averaging. We analyze the total ergotropy, its population and coherent contributions, the energy basis populations, a passive ordering violation diagnostic, and the Jensen–Shannon coherence of the noise-averaged state. The results show that resonant tunnel coupling driving selects a dominant $E_0 \leftrightarrow E_3$ population transfer channel in the interacting DQD spectrum. The dominant extractable work is stored in non-passive population distributions, in agreement with recent population ordering interpretations of ergotropy in QBs, while coherence accompanies and supports the resonant transfer as a transient dynamical resource. Detuning noise reduces the energy basis coherence amplitude and also weakens the population transfer pathway responsible for the dominant population ergotropy. This framework provides a noise aware description of semiconductor QB charging based on extractable work rather than on injected energy alone.

I. INTRODUCTION

QBs provide a microscopic framework for studying energy storage, charging dynamics, and extractable work in finite dimensional quantum systems. In contrast to classical batteries, where energy storage is governed by macroscopic electrochemical processes, QBs can store energy through coherent evolution, population redistribution, and correlations between elementary quantum units. Their useful performance is most naturally quantified by the ergotropy, namely the maximum work that can be extracted from a quantum state by unitary operations with respect to a fixed battery Hamiltonian. This distinction is essential because an increase in the mean energy does not necessarily imply an equivalent increase in extractable work [1–4]. A central question in QB physics is how quantum resources contribute to useful work storage [5–9]. Coherence and entanglement can modify the charging pathway, enhance power, or affect work extraction, but they do not by themselves determine the full ergotropy. Recent theoretical and experimental studies have shown that ergotropy can be separated into coherent and incoherent, or population based, contributions. In this view, useful work may originate either from energy basis coherences or from non-passive population distributions [10–12]. This distinction is particularly important in driven multilevel batteries, where a coherent drive may first create superpositions and then redistribute populations in a way that violates passive ordering.

Semiconductor quantum dots (QDs) offer a promising solid state platform for exploring such mechanisms because they combine strong confinement, fast electrical control, and compatibility with scalable semiconductor architectures [13, 14]. In particular, Si/SiGe QDs are attractive because silicon based architectures provide strong prospects for scalability and reduced nuclear spin noise compared with GaAs based platforms, while charge noise remains a central limitation for electrically controlled charge dynamics [13–16]. In a DQD, the localized charge states form an effective charge qubit, while the detuning and tunnel coupling provide two direct control axes. The detuning sets the relative energy of the localized charge configurations, whereas the tunnel coupling hybridizes them and opens an anticrossing. This makes DQDs natural platforms for coherent charge oscillations, microwave spectroscopy, Landau Zener physics, and electrically driven charge qubit dynamics [16–22]. Beyond isolated DQDs, capacitively coupled DQDs provide an additional ingredient that is highly relevant for QB applications: an electrically tunable interaction between charge qubits. Experiments have demonstrated microwave driven transitions, strong capacitive coupling between neighboring charge qubits, correlated charge oscillations, and conditional operations on sub nanosecond time scales [23–27]. In the localized charge basis, the capacitive interaction acts as a conditional electrostatic shift and is naturally represented by an effective Ising-type term proportional to $\sigma_z^{(1)}\sigma_z^{(2)}$. Such an interaction provides a minimal and experimentally motivated route to correlated charging dynamics in a two DQD QB. The same electric dipole moment that enables fast electrical control also makes charge states sensitive to electrostatic fluctuations. In gate defined semiconductor nanostructures, charge noise mainly

* khalil.loukhssami@um5r.ac.ma

† khadija_elhawary@um5.ac.ma

perturbs the detuning coordinate, thereby shifting the relative energy of the localized states. This type of noise is commonly associated with fluctuating charges, charge traps, interface disorder, electric dipoles, and ensembles of two level fluctuators, and it often displays a low frequency $1/f^\alpha$ spectrum [28–35]. Since detuning controls the alignment of the charge states, detuning noise can directly affect charge transfer, dephase charge qubit dynamics, and reduce the fidelity of charge motion between neighboring dots [36–41]. This point is especially important for the present work. Studies of charge transfer in QDs have shown that the basic transfer mechanism is governed by the competition between detuning control and interdot tunneling. The detuning determines which localized charge configuration is energetically favored, while the tunnel coupling controls the anticrossing through which charge is transferred. In realistic devices, fluctuations of detuning act as longitudinal noise and can degrade the transfer process. In many QD settings, detuning noise is therefore treated as the dominant charge noise channel, whereas tunnel coupling noise is often considered weaker or secondary [42]. This motivates our choice to charge the battery through tunnel coupling modulation while modeling the uncontrolled environment as stochastic detuning noise. The influence of $(1/f)$ detuning noise is subtle because its effect depends on the noise bandwidth and on the time scale of the driven operation. Low frequency components vary slowly during a microwave pulse and produce realization dependent shifts of the effective detuning and transition frequencies. Higher frequency components fluctuate during the pulse and may contribute to dynamical dephasing and resonance frequency fluctuations. Therefore, a noise aware description of a driven semiconductor QB should not be replaced, in general, by a single phenomenological Markovian decay rate. Band limited $1/f$ detuning noise contains slow components, which act as realization dependent frequency shifts over a charging pulse, as well as dynamical components that fluctuate during the driven evolution. Stochastic Hamiltonian simulations and cumulant expansion approaches are well suited to this situation because they retain the finite time correlations of the colored noise and can capture both Markovian like and non Markovian contributions to the noise-averaged dynamics [41, 43]. Microwave driving provides a possible route to robust operation because faster control can reduce the exposure time to slow charge noise and move the relevant dynamics toward higher frequencies where $(1/f)$ noise is weaker. However, strong driving may also introduce additional effects, including Bloch Siegert shifts, fast oscillations, leakage, and noise induced fluctuations of the Rabi frequency. Previous studies of charge and hybrid QD qubits have shown that robust operation can be improved by pulse engineering, synchronization of fast oscillations, and AC sweet spot strategies [43–45]. These results motivate the search for charging protocols that combine fast coherent transfer with reduced sensitivity to detuning noise. Despite this progress, experimentally motivated charge noise effects remain largely unexplored

in semiconductor QBs. In particular, it is not yet clear how band limited $(1/f)$ detuning noise modifies the decomposition of ergotropy into coherent and population-based contributions in a capacitively coupled DQD battery. This question is important because detuning noise can suppress energy basis coherence, but it can also distort the population transfer pathway that creates non-passive states. Consequently, the loss of extractable work cannot be interpreted solely as coherence decay. In this work, we develop a noise aware model of a capacitively coupled DQD QB driven by resonant microwave modulation of the tunnel coupling channel. The static battery Hamiltonian is chosen from experimentally motivated Si/SiGe charge qubit parameters, and the operating point is placed at the symmetric zero detuning point. Detuning fluctuations are modeled as classical stochastic processes generated from a band limited $(1/f)$ spectrum. For each noise realization, the battery evolves unitarily, while decoherence and loss of contrast emerge only after ensemble averaging. We evaluate the total ergotropy, population ergotropy, coherent ergotropy, energy basis populations, a passive ordering violation diagnostic, and Jensen–Shannon coherence of the noise-averaged state. Our main goal is to identify how detuning charge noise affects the physical mechanism of useful work storage. We show that resonant tunnel coupling driving selects a dominant $E_0 \leftrightarrow E_3$ population transfer channel in the interacting DQD spectrum. The coherent drive generates energy basis coherence during the transfer, while the dominant extractable work is stored in non-passive population distributions. To make this mechanism explicit, we introduce a passive ordering violation indicator that directly tracks when the diagonal energy basis populations depart from passive ordering. Detuning noise therefore degrades the battery through two connected effects: it reduces the energy basis coherence amplitude generated by the drive and weakens the population ordering pathway responsible for the dominant population ergotropy. This framework connects ergotropy based QB performance with semiconductor charge qubit control and $(1/f)$ charge noise physics.

II. THEORETICAL MODEL

A. Static battery Hamiltonian

We consider a QB formed by two capacitively coupled DQDs, each operated in the charge qubit regime. For each DQD, the relevant low energy subspace is spanned by the localized charge states $|L\rangle$ and $|R\rangle$, corresponding to one excess electron occupying the left or right dot. The two DQD battery is therefore described in the localized product basis $|LL\rangle, |LR\rangle, |RL\rangle, |RR\rangle$. This basis is physically natural because the detuning coordinate couples to the electric dipole moment of each DQD, whereas the tunnel splitting controls the hybridization between localized charge configurations. Localized charge states of this form constitute the standard framework for describing

coherent charge oscillations, microwave spectroscopy, and electrically driven charge qubit dynamics in semiconductor DQDs [16, 20]. The static Hamiltonian of the coupled DQD battery is written as

$$H_B = \sum_{i=1}^2 \left[\frac{\epsilon_{0,i}}{2} \sigma_z^{(i)} + \frac{\Delta_{0,i}}{2} \sigma_x^{(i)} \right] + \frac{J}{4} \sigma_z^{(1)} \sigma_z^{(2)}. \quad (1)$$

Here, $\epsilon_{0,i}$ denotes the static detuning of the i th DQD, while $\Delta_{0,i} = 2t_c^{(i)}$ is the corresponding tunnel splitting, with $t_c^{(i)}$ the interdot tunnel coupling. In the following, we use $\Delta_{0,i}$ as the relevant tunnel splitting parameter. The parameter J denotes the capacitive Ising interaction strength between the two charge qubits, which produces a conditional electrostatic shift depending on the joint charge configuration of the coupled DQDs. The longitudinal term proportional to $\sigma_z^{(i)}$ controls the charge polarization of each DQD, whereas the transverse term proportional to $\sigma_x^{(i)}$ hybridizes the localized states and opens the anticrossing near zero detuning. The Ising term proportional to $\sigma_z^{(1)} \sigma_z^{(2)}$ accounts for the inter-DQD capacitive coupling and provides the interaction mechanism responsible for correlated charging dynamics. The competition between detuning, tunnel splitting, and capacitive Ising coupling is the basic mechanism behind coherent charge rotations, charge transfer, and interaction-assisted charging in coupled DQDs [25, 41].

The last term in Eq. (1) describes the capacitive interaction between the two charge qubits. In the localized charge basis, this interaction acts as a conditional electrostatic shift: the transition frequency of one DQD depends on the charge configuration of the other. Such capacitive coupling has been experimentally used to generate correlated charge dynamics and conditional operations in coupled charge qubit devices [24]. It therefore provides a minimal and experimentally motivated mechanism for producing correlated charging dynamics in a semiconductor QB. The eigenstates of H_B are denoted by $|\phi_n\rangle$, with eigenenergies ordered as $E_0 \leq E_1 \leq E_2 \leq E_3$. This energy eigenbasis is used throughout the paper as the reference basis for populations, coherences, passive states, and ergotropy. This choice is essential because the passive state construction, and therefore the extractable work, must be defined with respect to a fixed battery Hamiltonian. Unless otherwise stated, we use experimentally motivated Si/SiGe charge-qubit parameters, namely $\Delta_{0,1}/h = 8.4$ GHz, $\Delta_{0,2}/h = 6.6$ GHz, and $J/h = 15.3$ GHz, where h denotes Planck's constant, as reported in capacitively coupled Si/SiGe charge-qubit experiments [25, 46]. The static detunings are chosen at the symmetric operating point, $\epsilon_{0,1} = \epsilon_{0,2} = 0$. For an isolated DQD charge qubit, this zero detuning point corresponds to the charge degeneracy point and acts as a static detuning sweet spot, where the transition frequency is first order insensitive to detuning fluctuations [43]. In the coupled DQD battery, we use the same symmetric point as a noise reduced working point: it maximizes tunnel hybridization, gives large transition

matrix elements, and produces a well resolved interacting spectrum. This choice, however, should not be confused with a fully optimized AC sweet spot protocol. We do not tune the microwave phase, amplitude, or combined detuning tunnel modulation to cancel all drive induced noise channels. Instead, the purpose of the present work is to quantify how a selective resonant tunnel coupling charging protocol behaves under band limited $1/f$ detuning noise. Even at $\epsilon_{0,1} = \epsilon_{0,2} = 0$, stochastic detuning fluctuations can still perturb the driven dynamics through higher order detuning sensitivity, resonance frequency fluctuations, and ensemble averaged weakening of the population transfer pathway. In this regime, the tunnel splittings and the capacitive coupling are comparable energy scales. Consequently, the many body spectrum is not simply the sum of two independent DQD spectra. Instead, the capacitive interaction produces conditional branches and well resolved interacting transitions that can be selectively addressed by microwave driving.

B. Microwave charging through tunnel coupling modulation

The charging protocol is implemented by resonantly modulating the tunnel coupling channel. This choice is motivated by two complementary considerations. First, the tunnel coupling controls the hybridization between $|L\rangle$ and $|R\rangle$ and therefore provides a transverse control axis for inducing transitions between eigenstates of H_B . Second, the dominant uncontrolled electrical noise in gate defined DQDs mainly enters through the detuning coordinate, because detuning fluctuations shift the relative energy of the localized charge states [32, 39, 40]. Driving through the tunnel coupling channel therefore injects energy into the battery without intentionally modulating the noisiest control parameter. During the charging stage, the deterministic Hamiltonian is

$$H_0(t) = H_B + H_{\text{ch}}(t), \quad (2)$$

with

$$H_{\text{ch}}(t) = \sum_{i=1}^2 \frac{A_{\Delta,i}}{2} \cos(\omega_d t + \varphi_i) \sigma_x^{(i)}. \quad (3)$$

Here, $A_{\Delta,i}$ is the modulation amplitude of the tunnel splitting of DQD i , ω_d is the angular drive frequency, and φ_i is the drive phase. Unless otherwise stated, we consider in phase symmetric driving, $A_{\Delta,1} = A_{\Delta,2} \equiv A_{\Delta}$ and $\varphi_1 = \varphi_2 = 0$, so that

$$H_{\text{ch}}(t) = \frac{A_{\Delta}}{2} \cos(\omega_d t) \left(\sigma_x^{(1)} + \sigma_x^{(2)} \right). \quad (4)$$

This term is transverse in the localized charge basis. It does not shift the localized charge states directly; instead, it modulates the interdot hybridization and couples the eigenstates of the interacting battery Hamiltonian. Such

transverse microwave control is closely related to the strong driving protocols developed for charge and hybrid QD qubits [47]. The drive frequency is chosen from the static many body spectrum. A transition $|\phi_n\rangle \leftrightarrow |\phi_m\rangle$ is efficiently addressed when

$$\hbar\omega_d \simeq E_m - E_n \quad (5)$$

and when the corresponding tunnel drive matrix element

$$M_{mn}^{(\Delta)} = \langle \phi_m | \left(\sigma_x^{(1)} + \sigma_x^{(2)} \right) | \phi_n \rangle \quad (6)$$

is sufficiently large. Since the battery is initialized in the ground state $|\phi_0\rangle$, the relevant charging channels are the transitions $|\phi_0\rangle \rightarrow |\phi_m\rangle$ that combine a large energy gap with a large drive matrix element. In the main protocol, the microwave is tuned close to the dominant transition

$$f_d = \frac{E_3 - E_0}{h}, \quad \omega_d = 2\pi f_d. \quad (7)$$

This resonant protocol transfers population from the low energy sector to the high energy sector of the battery while generating energy basis coherences. The charging process is therefore neither a purely classical population pump nor a purely coherence storage process. Rather, the microwave field first creates coherent superpositions, and the subsequent driven dynamics can convert part of this coherence into a non-passive population distribution. This mechanism is important for QB operation because ergotropy can arise from both off diagonal coherences and violations of passive population ordering in the energy basis [5, 8, 11].

In the absence of charge noise, the density matrix evolves according to

$$\frac{d\rho_0(t)}{dt} = -\frac{i}{\hbar} [H_0(t), \rho_0(t)], \quad (8)$$

with $\rho_0(0) = |\phi_0\rangle\langle\phi_0|$. This ideal coherent evolution defines the reference charging dynamics. In the following, detuning fluctuations are introduced as a stochastic perturbation, and the resulting noise-averaged state is compared with this noiseless reference to quantify the degradation of population transfer, energy basis coherence, and ergotropy.

C. Detuning charge noise

Charge noise is one of the dominant limitations of electrically controlled semiconductor QDs. Its microscopic origin is generally associated with slow electrostatic fluctuations in the device environment, including background charges, charge traps, interface disorder, remote impurities, and fluctuating two level systems [28–30]. In gate defined DQDs, these fluctuations couple most directly to the detuning coordinate, because the localized charge states $|L\rangle$ and $|R\rangle$ have different electric dipole moments.

A fluctuation of the local electrostatic potential therefore appears as a stochastic shift of the energy bias between the two dots [36, 39].

In the present battery protocol, this mechanism plays a particularly important role. The coherent charging field is applied through the tunnel coupling channel, whereas the dominant uncontrolled electrical noise is assumed to perturb the detuning coordinates. We therefore write the instantaneous detuning of the i th DQD as $\epsilon_i(t) = \epsilon_{0,i} + \delta\epsilon_i(t)$, where $\epsilon_{0,i}$ is the chosen static operating point and $\delta\epsilon_i(t)$ is a classical stochastic fluctuation. The corresponding noise Hamiltonian is [32, 35]

$$H_n(t) = \sum_{i=1}^2 \frac{\delta\epsilon_i(t)}{2} \sigma_z^{(i)}. \quad (9)$$

Thus, detuning noise is longitudinal in the localized charge basis. However, its effect on the battery dynamics is not limited to a simple phase fluctuation. Since the static Hamiltonian contains tunnel coupling terms proportional to $\sigma_x^{(i)}$, and since the system is driven during the charging stage, $H_n(t)$ does not generally commute with $H_B + H_{\text{ch}}(t)$. Consequently, detuning noise can suppress energy basis coherences, shift the resonance condition, and modify the population transfer pathway between the eigenstates of the interacting battery Hamiltonian.

For a given noise realization α , the total Hamiltonian is

$$H_\alpha(t) = H_B + H_{\text{ch}}(t) + \sum_{i=1}^2 \frac{\delta\epsilon_i^{(\alpha)}(t)}{2} \sigma_z^{(i)}. \quad (10)$$

The stochastic processes $\delta\epsilon_i(t)$ are taken to have zero mean and stationary correlations. Unless otherwise stated, the two local detuning noises are considered independent and statistically identical. This assumption provides the minimal model for local charge noise induced degradation. Spatially correlated noise could be included by introducing nonzero cross correlations between $\delta\epsilon_1(t)$ and $\delta\epsilon_2(t)$, but this extension is not required for the present analysis.

Following standard models of low frequency charge noise in semiconductor nanostructures, we describe the detuning fluctuations by a band limited $1/f$ spectrum [30, 32, 43]. Using the angular frequency convention, the noise power spectrum inside the finite bandwidth is written as

$$\tilde{S}_\epsilon(\omega) = \begin{cases} \frac{2\pi c_\epsilon^2}{|\omega|}, & \omega_l \leq |\omega| \leq \omega_h, \\ 0, & \text{otherwise.} \end{cases} \quad (11)$$

Here, c_ϵ controls the spectral noise strength, while ω_l and ω_h are the low and high angular frequency cutoffs defining the finite noise bandwidth. Throughout the noise model we use angular frequencies, with $\omega = 2\pi f$. It is important to distinguish the spectral amplitude c_ϵ from the time domain root mean square (RMS) detuning fluctuation. With the two sided angular frequency convention used in

Eq. (11), the RMS fluctuation integrated over the finite bandwidth is

$$\sigma_\epsilon^2 = 2c_\epsilon^2 \ln(\omega_h/\omega_l). \quad (12)$$

Thus, c_ϵ is the parameter that fixes the amplitude of the band limited $1/f$ spectrum used to generate the stochastic detuning traces, whereas σ_ϵ is a bandwidth dependent RMS quantity obtained after integrating that spectrum. In the figures below, the noise strength is therefore labeled by c_ϵ , which is the scanned simulation parameter, and not by σ_ϵ . The latter is quoted only as an equivalent RMS scale for the chosen frequency window. We do not assign a universal value to c_ϵ , since charge noise amplitudes depend strongly on the material stack, device geometry, gate configuration, and operating point. Instead, c_ϵ is treated as a tunable spectral parameter that allows us to quantify the robustness of the charging protocol over a controlled range of detuning noise strengths.

The finite bandwidth in Eq. (11) has a direct physical meaning. Low frequency components of the generated $1/f$ traces vary slowly on the time scale of a single microwave charging pulse and therefore produce realization dependent shifts of the effective detuning and transition frequencies. Higher frequency components fluctuate during the pulse and contribute to dynamical dephasing, resonance frequency fluctuations, and drive noise crosstalk. Thus, the same band limited $1/f$ trace contains both slowly varying and dynamically fluctuating components. In the simulations, we do not introduce an additional independent quasi-static disorder term. Each realization is instead described by a single stochastic trace $\delta\epsilon_i^{(\alpha)}(t)$ generated from the band limited $1/f$ spectrum of Eq. (11). In practice, the colored detuning traces are generated using a Fourier synthesis procedure. For each realization, random Fourier components are assigned according to the spectral density in Eq. (11), with phases chosen randomly and amplitudes chosen to reproduce the prescribed noise power spectrum. An inverse Fourier transform then gives the stochastic detuning trace $\delta\epsilon_i^{(\alpha)}(t)$. For each realization, the system evolves unitarily under $H_\alpha(t)$, and the experimentally relevant noisy state is obtained only after ensemble averaging over many independent noise realizations. The use of a classical stochastic description is appropriate for the low frequency charge noise environment considered here. Although microscopic fluctuators may be non Gaussian when a single fluctuator is strongly coupled to the device, the combined effect of many weak fluctuators is commonly approximated by a Gaussian process with a prescribed power spectral density [32, 41]. This approximation is also consistent with numerical studies of driven QD qubits, where detuning noise traces are generated from a $1/f$ spectrum and the quantum dynamics is averaged over many stochastic realizations.

D. Noise-averaged dynamics

The dynamics in the presence of charge noise is treated using a stochastic Hamiltonian approach. The detuning fluctuations are modeled as classical random processes, while the quantum state evolves coherently for each fixed noise realization. This semiclassical treatment is appropriate for low frequency charge noise in semiconductor nanostructures, where the environment is represented by stochastic detuning traces with a prescribed power spectral density [43].

For a given realization α , the density matrix obeys

$$\frac{d\rho_\alpha(t)}{dt} = -\frac{i}{\hbar} [H_\alpha(t), \rho_\alpha(t)]. \quad (13)$$

Each trajectory is therefore unitary. Decoherence appears only after averaging over statistically independent realizations, because different trajectories accumulate different noise induced phases and follow slightly different population transfer pathways. The noise-averaged state is defined as

$$\rho(t) = \frac{1}{N_r} \sum_{\alpha=1}^{N_r} \rho_\alpha(t), \quad (14)$$

where N_r is the number of stochastic realizations used in the numerical average.

All battery observables are evaluated from the averaged state $\rho(t)$. This choice is important: ergotropy, population ergotropy, coherent ergotropy, and energy basis coherence are computed after the ensemble average, because $\rho(t)$ is the physical state obtained when the specific noise realization is not known experimentally. In this way, the loss of contrast in populations and coherences directly reflects the experimentally observable effect of detuning noise.

The same propagation scheme is used for the noiseless reference dynamics and for the time-dependent band limited $1/f$ noise model. In the noisy case, each trajectory contains a colored time-dependent detuning trace generated from Eq. (11). This trajectory based procedure keeps the full time dependence of both the microwave drive and the detuning fluctuations, without imposing a Markov approximation.

E. Extractable work observables and ergotropy decomposition

All extractable work observables are evaluated from the noise-averaged state $\rho(t)$ with respect to the static battery Hamiltonian H_B . In this work, the central performance quantity is the ergotropy, which measures the part of the battery energy that can be extracted by a unitary operation. This choice is important for a noisy driven multilevel system because a large energy expectation value does not necessarily imply a large amount of useful work.

The total ergotropy is defined as [48, 49]

$$\xi(t) = \text{Tr}[H_B \rho(t)] - \text{Tr}[H_B \pi(t)], \quad (15)$$

where $\pi(t)$ is the passive state associated with $\rho(t)$. The passive state is constructed by assigning the eigenvalues of $\rho(t)$, ordered from largest to smallest, to the eigenstates of H_B , ordered from lowest to highest energy, following the standard passivity construction [50, 51]. Thus, $\xi(t)$ directly quantifies the useful work stored in the state after ensemble averaging over the detuning noise realizations.

To identify the physical origin of the extractable work, we separate the ergotropy into population and coherent contributions [52]. We first dephase the state in the energy eigenbasis of H_B ,

$$\rho_d(t) = \sum_k \langle \phi_k | \rho(t) | \phi_k \rangle | \phi_k \rangle \langle \phi_k |. \quad (16)$$

The population ergotropy is then defined as the ergotropy of this dephased state,

$$\xi_P(t) = \text{Tr}[H_B \rho_d(t)] - \text{Tr}[H_B \pi_d(t)], \quad (17)$$

where $\pi_d(t)$ is the passive state associated with $\rho_d(t)$. The coherent contribution is obtained by subtraction,

$$\xi_C(t) = \xi(t) - \xi_P(t). \quad (18)$$

The population contribution $\xi_P(t)$ measures the extractable work stored in the diagonal energy basis populations, namely in non-passive population orderings. By contrast, $\xi_C(t)$ measures the additional extractable work that is lost when the state is dephased in the energy basis. Thus, $\xi_C(t)$ is associated with energy basis coherences, whereas $\xi_P(t)$ is associated with non-passive population orderings, including but not limited to population inversion. The population contribution has a direct passivity interpretation. In the energy eigenbasis of H_B , the diagonal populations are

$$p_n(t) = \langle \phi_n | \rho(t) | \phi_n \rangle, \quad E_0 \leq E_1 \leq E_2 \leq E_3. \quad (19)$$

Since $\rho_d(t)$ is diagonal in this basis, its ergotropy is entirely determined by the ordering of the populations. For the non degenerate spectrum considered here, the dephased state $\rho_d(t)$ is passive if and only if

$$p_0(t) \geq p_1(t) \geq p_2(t) \geq p_3(t). \quad (20)$$

Consequently, $\xi_P(t) > 0 \iff \rho_d(t)$ is non passive. Indeed, if the populations satisfy Eq. (20), then $\rho_d(t)$ is already passive and $\pi_d(t) = \rho_d(t)$, so that $\xi_P(t) = 0$. Conversely, if there exists a pair $n < m$ such that $p_m(t) > p_n(t)$, then the higher energy level E_m is more populated than the lower energy level E_n . Exchanging these two populations decreases the energy by

$$\Delta U_{nm} = (E_m - E_n) [p_m(t) - p_n(t)] > 0, \quad (21)$$

which shows that the diagonal state is non-passive and that a finite amount of work can be extracted from the

population ordering. Therefore, the population ergotropy is positive exactly when the diagonal energy basis populations violate passive ordering.

To visualize this mechanism, we introduce the passive ordering violation indicator

$$\mathcal{V}_{\text{pass}}(t) = \sum_{0 \leq n < m \leq 3} (E_m - E_n) [p_m(t) - p_n(t)]_+, \quad (22)$$

where $[x]_+ = \max(x, 0)$. This quantity is zero when the diagonal state is passive and becomes positive whenever at least one pair of populations violates the passive ordering. It is therefore a diagnostic of the same non passivity condition that gives $\xi_P(t) > 0$. In particular, it detects partial violations such as $p_3 > p_1$ or $p_3 > p_2$, even when the stronger highest-lowest inversion condition $p_3 > p_0$ is not yet satisfied. However, $\mathcal{V}_{\text{pass}}(t)$ should not be interpreted as an additional ergotropy contribution. In general, $\mathcal{V}_{\text{pass}}(t) \neq \xi_P(t)$, because $\mathcal{V}_{\text{pass}}$ sums all pairwise ordering violations, whereas ξ_P is obtained from the globally passive rearrangement of $\rho_d(t)$. Thus, $\mathcal{V}_{\text{pass}}$ is used only to identify and visualize the population ordering pathway responsible for the population ergotropy.

In the present resonant protocol, the microwave tunnel drive first generates coherent superpositions between battery eigenstates and then converts part of this coherent dynamics into population redistribution. Coherence is therefore not treated only as a static storage channel. It also accompanies the resonant transfer and supports the formation of non-passive population orderings. Under detuning noise, both mechanisms may be affected: energy basis coherences are suppressed by dephasing, while the population transfer pathway can be distorted by stochastic detuning fluctuations.

F. Jensen–Shannon coherence

Quantum coherence is basis dependent and quantifies the ability of a quantum state to form superpositions with respect to a chosen reference basis [53, 54]. In this work, coherence is evaluated in the energy eigenbasis of the static battery Hamiltonian H_B . This is the natural basis for the present analysis because passive states, ergotropy, and population ergotropy are all defined with respect to the same Hamiltonian.

For the noise-averaged state $\rho(t)$, the corresponding incoherent state is obtained by removing all off diagonal elements in the energy eigenbasis of H_B . This state is precisely $\rho_d(t)$, defined in Eq. (16). The difference between $\rho(t)$ and $\rho_d(t)$ therefore measures the amount of energy basis coherence generated during the charging process.

To quantify this coherence, we use the quantum Jensen–Shannon divergence, which provides a symmetric and bounded distinguishability measure between two quantum

states [55–57]. It is defined as

$$J(\rho(t), \rho_d(t)) = S\left[\frac{\rho(t) + \rho_d(t)}{2}\right] - \frac{1}{2}S[\rho(t)] - \frac{1}{2}S[\rho_d(t)], \quad (23)$$

where

$$S(\rho) = -\text{Tr}[\rho \log_2 \rho] \quad (24)$$

is the von Neumann entropy. The logarithm is taken in base 2 in the numerical calculations. The Jensen–Shannon coherence is then defined as

$$C_{\text{JS}}(t) = \sqrt{J(\rho(t), \rho_d(t))}. \quad (25)$$

The quantity $C_{\text{JS}}(t)$ measures the distance between the noise-averaged battery state and its energy dephased counterpart. It is particularly useful for the present problem because it remains well defined for mixed states, including the ensemble averaged states generated by band limited $1/f$ detuning noise. Importantly, $C_{\text{JS}}(t)$ is not identified with the total ergotropy. Instead, it is analyzed together with $\xi(t)$, $\xi_P(t)$, $\xi_C(t)$, and $\mathcal{V}_{\text{pass}}(t)$ in order to determine whether useful work is stored mainly in energy basis coherence or in non-passive populations.

III. RESULTS AND DISCUSSION

A. Spectral selection and noise-averaged coherent charging

The static spectrum and the corresponding noise-averaged driven dynamics are summarized in Fig. 1. The spectrum is used to identify the working point and the transition addressed by the tunnel coupling modulation. The dynamical panels then compare the ideal coherent evolution with the ensemble averaged evolution under detuning noise. The results in Fig. 1 first identify the physical charging channel of the device. The static spectrum in Fig. 1 (a) defines the energy eigenbasis used throughout the analysis and shows the transition structure selected at the operating point. In the present protocol, Fig. 1 (b), the microwave tunnel coupling modulation is chosen to address the dominant $E_0 \leftrightarrow E_3$ transition. This choice is confirmed dynamically by the complementary oscillations of $p_0(t)$ and $p_3(t)$. The finite noise curves preserve the same qualitative transfer mechanism, but their reduced contrast shows that detuning fluctuations degrade the visibility of the coherent population exchange. The coherence dynamics shows that the charge transfer is not a purely classical population process in the energy eigenbasis. The Jensen–Shannon coherence Fig. 1 (c) remains finite during the charging dynamics, which means that the microwave drive creates superpositions in the energy eigenbasis. However, the coherence amplitude is partially suppressed by the noise-averaged detuning fluctuations. Thus, the role of charge noise is twofold: it reduces the energy basis coherence amplitude generated by the drive

and, through ensemble averaging over different stochastic trajectories, it also weakens the observable population transfer contrast. This behavior is consistent with a semi-classical noise picture in which each realization evolves unitarily, while dephasing appears only after averaging over many noise traces.

B. Population dominated ergotropy and passive ordering violation

The ergotropy decomposition and the coherence population ordering pathway are shown in Fig. 2. The aim of this analysis is twofold. First, we identify which part of the ergotropy is stored in the diagonal energy basis populations and which part is associated with energy basis coherences. Second, we clarify the passive ordering mechanism responsible for the dominance of the population contribution in the present resonant charging protocol. Figure 2(a) shows that the total ergotropy $\xi(t)$ (Eq. (15)) follows the population contribution $\xi_P(t)$ (Eq. (17)) much more closely than the coherent contribution $\xi_C(t)$ (Eq. (18)). This indicates that, for the present protocol, the dominant part of the extractable work is stored in the diagonal population structure of the battery state. In contrast, the coherent contribution remains comparatively small over the first charging branch. This result should not be interpreted as an absence of coherence. The finite Jensen–Shannon coherence confirms that the resonant microwave drive does generate superpositions in the energy eigenbasis of H_B . Rather, the decomposition shows that this coherence is not the dominant final storage channel of ergotropy for the selected $E_0 \leftrightarrow E_3$ charging pathway. The parametric trajectories in Figs. 2(b) and 2(c) identify the population ordering mechanism behind the dominance of ξ_P . The horizontal coordinate C_{JS} tracks the energy basis coherence, while $I_{03} = p_3 - p_0$ measures the population imbalance between the highest and lowest energy levels. According to the passivity criterion established in Sec. II E, $\xi_P(t)$ becomes positive exactly when the dephased state $\rho_d(t)$ is non passive, namely when the energy basis populations violate the passive ordering $p_0 \geq p_1 \geq p_2 \geq p_3$. Therefore, population ergotropy can become finite before the highest-lowest threshold $p_3 > p_0$ is reached. A partial violation, such as $p_3 > p_1$ or $p_3 > p_2$, is already sufficient to make the diagonal state non-passive and hence to allow a nonzero population ergotropy. This explains the separation between the two markers in Fig. 2(b). The first marker, $\mathcal{V}_{\text{pass}} > 0$, indicates the onset of non passivity of $\rho_d(t)$ and therefore the relevant threshold for $\xi_P(t) > 0$. The second marker, $p_3 > p_0$, corresponds only to the stronger highest-lowest inversion condition. Thus, the resonant drive can generate population ergotropy before the highest-lowest inversion threshold is reached. The trajectory color coded by ξ_P/ξ in Fig. 2(c) confirms that, once the diagonal populations become non passive, most of the extractable work is carried by the population channel. This interpretation is consistent with coherence

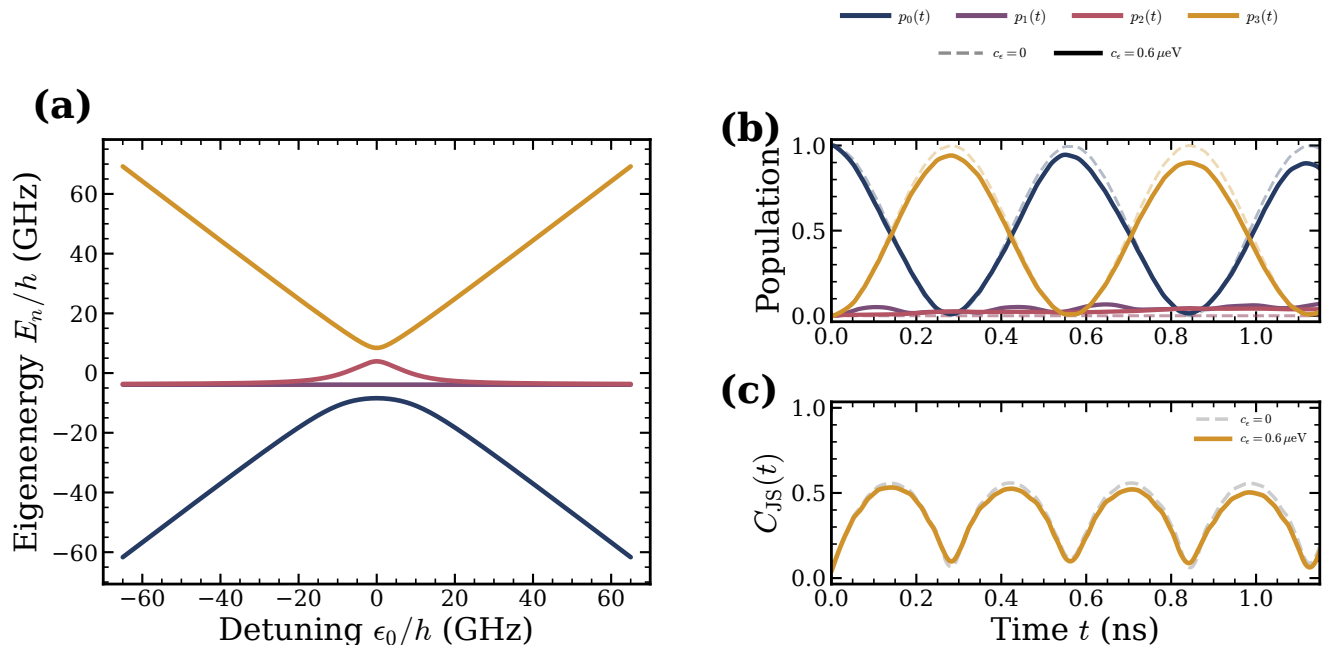


FIG. 1. Static spectrum and noise-averaged microwave driven charging dynamics of the capacitively coupled DQD. (a) Eigenenergies E_n/h of the static battery Hamiltonian H_B as a function of the common dc detuning $\epsilon_{0,1}/h = \epsilon_{0,2}/h \equiv \epsilon_0/h$. The spectrum is calculated for $\Delta_{0,1}/h = 8.4$ GHz, $\Delta_{0,2}/h = 6.6$ GHz, and $J/h = 15.3$ GHz. The charging protocol is operated near the symmetric working point $\epsilon_0 = 0$, where the tunnel hybridization is strong and the interacting many body transition structure is well resolved. At this working point, the static eigenenergies are approximately $E_0/h = -8.419$ GHz, $E_1/h = -3.929$ GHz, $E_2/h = 3.929$ GHz, and $E_3/h = 8.419$ GHz, giving the dominant highest-lowest transition frequency $f_{03} = (E_3 - E_0)/h \simeq 16.838$ GHz. (b) Time evolution of the energy basis populations $p_n(t) = \langle \phi_n | \rho(t) | \phi_n \rangle$. The battery is initially prepared in $|\phi_0\rangle$ and charged by a resonant tunnel splitting microwave modulation with amplitude $A_\Delta/h = 4.0$ GHz and drive frequency $f_d = f_{03}$. The dynamics is dominated by complementary oscillations of $p_0(t)$ and $p_3(t)$, while the intermediate populations $p_1(t)$ and $p_2(t)$ remain weak. This confirms that the first charging branch is mainly governed by an effective $E_0 \leftrightarrow E_3$ population transfer channel embedded in the four level coupled DQD spectrum. (c) Jensen-Shannon coherence $C_{JS}(t)$ computed in the same energy eigenbasis of H_B . The noiseless dynamics is compared with the ensemble averaged dynamics at the representative spectral noise amplitude parameter $c_e = 0.6 \mu\text{eV}$. The stochastic detuning traces are generated from the band limited $1/f$ spectrum of Eq. (11), with angular frequency cutoffs $\omega_l/2\pi = 1$ Hz and $\omega_h/2\pi = 256$ GHz. At this representative noise strength, the dominant resonant charging pathway remains visible, while detuning noise reduces the population transfer contrast and the energy basis coherence amplitude after ensemble averaging.

based bounds on QB charging, where the stored work and charging power are controlled by the non commutativity between the battery Hamiltonian, the driving interaction, and the evolving state [6]. In the present two DQD battery, the tunnel coupling drive does not commute with the static battery Hamiltonian H_B , and therefore it can generate energy basis coherence and induce resonant population transfer. However, Fig. 2 shows that the coherence produced during the transfer is not the main final repository of extractable work. Instead, coherence accompanies the resonant transfer and supports the formation of non-passive population orderings, while the useful ergotropy is predominantly accumulated when the diagonal state becomes non passive. The two diagnostics therefore reveal complementary aspects of the same charging mechanism. The finite value of C_{JS} shows that the drive is genuinely coherent, whereas the large value of ξ_P/ξ shows that the dominant stored ergotropy is population based. This conclusion is specific to the

selective $E_0 \leftrightarrow E_3$ protocol considered here, in which the intermediate levels remain weakly populated. A different multilevel drive that strongly involves E_1 and E_2 could lead to a different balance between coherent and population ergotropy.

C. Noise induced weakening of the passive ordering pathway

The channel resolved ergotropy maps under detuning noise are shown in Fig. 3. The purpose of this figure is to identify which part of the charging mechanism is most affected by charge noise fluctuations. We compare the total ergotropy ξ , the population ergotropy ξ_P , the coherent ergotropy ξ_C , and the passive ordering violation indicator $\mathcal{V}_{\text{pass}}$. Here, $\mathcal{V}_{\text{pass}}(t, c_e)$ is computed from the energy basis populations of the noise-averaged state and detects violations of passive ordering in the diagonal

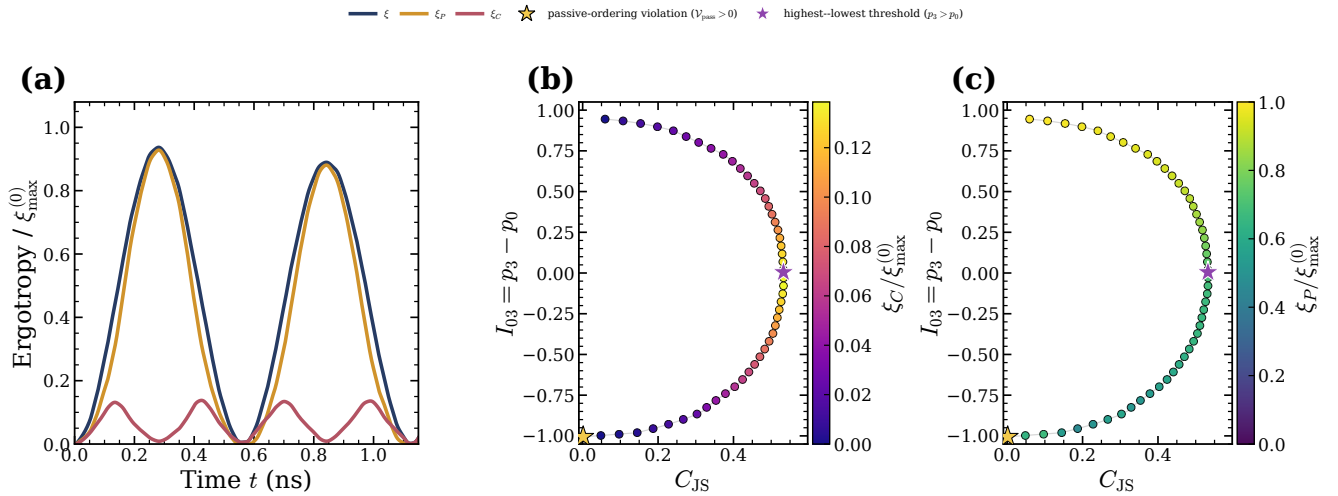


FIG. 2. Ergotropy decomposition and passive ordering pathway under band limited $1/f$ detuning noise. All panels are computed for the same static and driving parameters as in Fig. 1, namely $\Delta_{0,1}/h = 8.4$ GHz, $\Delta_{0,2}/h = 6.6$ GHz, $J/h = 15.3$ GHz, $A_\Delta/h = 4.0$ GHz, and $f_d = f_{03}$. The noisy dynamics corresponds to the representative spectral noise amplitude parameter $c_\epsilon = 0.6$ μeV , with angular frequency cutoffs $\omega_l/2\pi = 1$ Hz and $\omega_h/2\pi = 256$ GHz. (a) Time evolution of the total ergotropy $\xi(t)$, population ergotropy $\xi_P(t)$, and coherent ergotropy $\xi_C(t)$, normalized by the noiseless maximum $\xi_{\text{max}}^{(0)} = \max_t \xi(t, 0)$. (b) First charging branch in the (C_{JS}, I_{03}) plane, where $I_{03} = p_3 - p_0$ measures the highest-lowest population imbalance within the dominant $E_0 \leftrightarrow E_3$ charging channel. The color scale represents $\xi_C/\xi_{\text{max}}^{(0)}$. The first marker indicates the onset of passive ordering violation, identified by $\mathcal{V}_{\text{pass}} > 0$, while the second marker indicates the stronger highest-lowest inversion condition $p_3 > p_0$. The condition $\mathcal{V}_{\text{pass}} > 0$ marks the onset of non passivity of the dephased state $\rho_d(t)$ and is therefore the relevant population ordering threshold for $\xi_P(t) > 0$, whereas $p_3 > p_0$ is only the stronger highest-lowest inversion threshold within the dominant transfer channel. (c) Same trajectory color coded by the population fraction ξ_P/ξ . The large values of ξ_P/ξ show that the extractable work is mainly population based, even though the resonant dynamics generates finite energy basis coherence. The ratio ξ_P/ξ is evaluated only when the total ergotropy is above a small numerical threshold, in order to avoid artificial enhancement when ξ is negligible.

population distribution. Since $\mathcal{V}_{\text{pass}} > 0$ is equivalent to the non passivity of the dephased state $\rho_d(t)$, it identifies the time noise region where population ergotropy can be generated. It should nevertheless be interpreted as a diagnostic of passive ordering violation, and not as an additional ergotropy contribution, because in general $\mathcal{V}_{\text{pass}} \neq \xi_P$. Therefore, it provides a direct diagnostic of the non-passive population pathway responsible for the dominant population ergotropy.

Panels (a) and (b) exhibit very similar structures in the (t, c_ϵ) plane. The region of large total ergotropy appears in the same time window as the region of large population ergotropy, namely during the main charging branch around the maximum population transfer. This shows that the extractable work stored by the battery is predominantly governed by the diagonal population distribution in the energy eigenbasis. In other words, the total ergotropy follows the population channel much more closely than the coherent channel.

Panel (c) shows that the coherent ergotropy $\xi_C(t, c_\epsilon)$ remains finite over the explored noise range, but this should not be interpreted as noise insensitivity. Because this panel is displayed with a zoomed color scale, its absolute magnitude must be compared with the dominant population contribution in panel (b). The magnitude of ξ_C remains much smaller than the population contribu-

tion. Therefore, the coherent component is not absent; rather, it plays a transient dynamical role in the driven transfer. It accompanies the resonant transfer between energy eigenstates, but it is not the main final storage channel of extractable work in the present protocol.

The microscopic mechanism behind this population dominated behavior is clarified by panel (d). The map of $\mathcal{V}_{\text{pass}}(t, c_\epsilon)$ shows where the diagonal energy basis populations violate passive ordering. Since $\xi_P(t) > 0$ exactly when $\rho_d(t)$ is non passive, the overlap between the high $\mathcal{V}_{\text{pass}}$ region and the high ξ_P region gives a direct dynamical visualization of the passivity mechanism. Its structure closely follows the map of $\xi_P(t, c_\epsilon)$, confirming that the dominant population ergotropy is associated with non-passive population orderings. If the contour $p_3 = p_0$ is shown, it should be understood only as the threshold for the strongest highest-lowest inversion within the dominant $E_0 \leftrightarrow E_3$ charging channel. However, the passive ordering indicator is more general than this contour: it also detects partial violations, such as a higher excited level becoming more populated than an intermediate lower level, even when the highest-lowest inversion threshold is not yet reached.

As the detuning noise amplitude c_ϵ increases, the high $\mathcal{V}_{\text{pass}}$ region becomes weaker and less extended. This means that the noise progressively suppresses the abil-

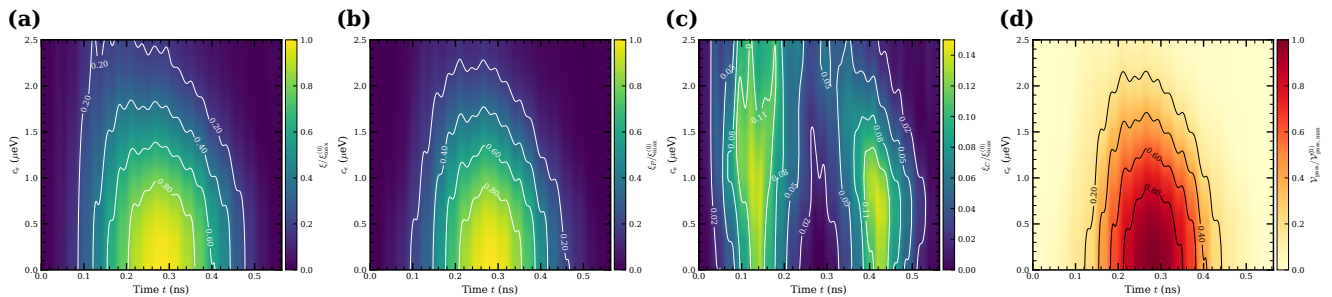


FIG. 3. Two dimensional ergotropy channel maps under band limited $1/f$ detuning charge noise during the first charging branch. All panels are computed for the same static and driving parameters as in Figs. 1 and 2, namely $\Delta_{0,1}/h = 8.4$ GHz, $\Delta_{0,2}/h = 6.6$ GHz, $J/h = 15.3$ GHz, $A_\Delta/h = 4.0$ GHz, and $f_d = f_{03}$. The stochastic detuning traces are generated from the band limited $1/f$ spectrum of Eq. (11), with angular frequency cutoffs $\omega_l/2\pi = 1$ Hz and $\omega_h/2\pi = 256$ GHz. The spectral noise amplitude parameter c_ϵ is varied from 0 to 2.5 μeV , as shown on the vertical axis. (a) Normalized total ergotropy $\xi(t, c_\epsilon)/\xi_{\max}^{(0)}$. (b) Normalized population ergotropy $\xi_P(t, c_\epsilon)/\xi_{\max}^{(0)}$. (c) Normalized coherent ergotropy $\xi_C(t, c_\epsilon)/\xi_{\max}^{(0)}$, displayed with a zoomed color scale. (d) Normalized passive ordering violation indicator $\mathcal{V}_{\text{pass}}(t, c_\epsilon)/\mathcal{V}_{\text{pass,max}}^{(0)}$. This panel identifies the region where the energy basis populations of the noise-averaged state violate passive ordering, and therefore visualizes the population ordering pathway associated with the dominant population ergotropy. Panels (a) to (c) are normalized by the noiseless maximum total ergotropy $\xi_{\max}^{(0)} = \max_t \xi(t, 0)$, whereas panel (d) is normalized by $\mathcal{V}_{\text{pass,max}}^{(0)} = \max_t \mathcal{V}_{\text{pass}}(t, 0)$.

ity of the resonant drive to build and maintain a non-passive population distribution. Since the total ergotropy is mainly population dominated, the reduction of $\xi(t, c_\epsilon)$ follows the reduction of $\xi_P(t, c_\epsilon)$, which in turn follows the weakening of the passive ordering violation measured by $\mathcal{V}_{\text{pass}}(t, c_\epsilon)$. This establishes the central message of Fig. 3: detuning noise reduces the useful ergotropy primarily by degrading the population ordering pathway that creates non-passive states, rather than by suppressing only the coherent contribution. This behavior can be understood in the same physical spirit as charge noise induced inhomogeneous dephasing in gate defined QDs [39]. Low frequency detuning fluctuations produce realization dependent shifts of the transition frequencies. In the present battery protocol, these fluctuations perturb the resonant $E_0 \leftrightarrow E_3$ charging channel and reduce the efficiency with which coherent driven motion is converted into a non-passive population ordering. The consequence is not simply a suppression of the coherent ergotropy, as panel (c) shows, but rather a degradation of the population ordering pathway that carries the dominant extractable work. Therefore, the main conclusion of Fig. 3 is that detuning noise does not simply destroy the coherent component of the dynamics. Within the present protocol, the visible loss of useful ergotropy is associated primarily with the weakening of the non-passive population transfer pathway, together with the reduction of the energy-basis coherence that accompanies the transfer. The dependence on c_ϵ also gives a direct materials oriented interpretation of the noise maps. Reducing the detuning noise amplitude is expected to enlarge the high ξ_P and high $\mathcal{V}_{\text{pass}}$ regions, thereby improving the robustness of the population ordering pathway responsible for the dominant extractable work. This interpretation is consistent with recent experimental progress in optimized $^{28}\text{Si}/\text{SiGe}$ QDs, where the use of thin silicon quantum wells and improved heterostructure design has

been shown to reduce low frequency charge noise [58]. Thus, Fig. 3 connects the QB degradation mechanism to an experimentally actionable route: lowering detuning charge noise through materials and device stack optimization should protect not only energy basis coherence, but also the non-passive population ordering pathway that carries the dominant ergotropy.

IV. CONCLUSION

In this work, we present a stochastic Hamiltonian description of a capacitively coupled DQD QB driven by resonant tunnel coupling modulation under experimentally motivated detuning charge noise. The static battery Hamiltonian is chosen from Si/SiGe charge qubit parameters, with tunnel splittings $\Delta_{0,1}/h = 8.4$ GHz and $\Delta_{0,2}/h = 6.6$ GHz, and capacitive coupling $J/h = 15.3$ GHz. Detuning fluctuations are included as classical time-dependent stochastic processes generated from a band limited $1/f$ spectrum, allowing the model to capture ensemble averaged loss of contrast induced by charge noise without introducing an additional quasi-static disorder model. The results show that resonant tunnel coupling driving induces coherent population transfer mainly between the lowest and highest energy levels of the interacting DQD spectrum. This identifies the $E_0 \leftrightarrow E_3$ transition as the dominant charging pathway during the first charging branch. Detuning noise reduces the visibility of this transfer and reduces the Jensen–Shannon coherence amplitude in the energy eigenbasis. However, the degradation of extractable work performance cannot be interpreted solely as coherence decay. Since detuning noise does not generally commute with the driven battery Hamiltonian, it also perturbs the population transfer path-

way that generates non-passive states. By decomposing the ergotropy into population and coherent contributions, we show that the dominant extractable work in the considered protocol is stored in the population contribution ξ_P . We establish that $\xi_P(t)$ is positive exactly when the dephased energy basis state $\rho_d(t)$ is non passive. The passive ordering indicator $\mathcal{V}_{\text{pass}}$ is therefore used as a diagnostic of this non passivity, not as an additional ergotropy contribution. The coherent contribution ξ_C remains finite and physically relevant, but it accompanies the resonant transfer and supports the formation of non-passive population orderings rather than as the principal storage channel of useful work. The parametric analysis in the (C_{JS}, I_{03}) plane further shows that population ergotropy can emerge from passive ordering violations, identified by $\mathcal{V}_{\text{pass}} > 0$, before the stronger highest-lowest threshold $p_3 > p_0$ is reached. This result clarifies why useful ergotropy may appear before the highest-lowest inversion threshold is established. The two dimensional noise maps provide a channel resolved picture of how detuning noise degrades the charging mechanism. The maps of $\xi(t, c_\epsilon)$ and $\xi_P(t, c_\epsilon)$ display closely related structures, confirming the population dominated character of the useful ergotropy in the present protocol. At the same time, the map of $\mathcal{V}_{\text{pass}}(t, c_\epsilon)$ shows that increasing detuning noise amplitude weakens the passive ordering violation region of the diagonal energy basis populations. Therefore, within this charging protocol, the visible loss of useful ergotropy is associated not only with the reduction of transient coherence, but more generally with the degradation of the non-passive population ordering pathway responsible for ξ_P . These results connect three ingredients that are usually treated separately: ergotropy based QB performance, semiconductor charge qubit control, and low frequency charge noise physics. They show that coherence should not be viewed only as a stored work resource. In this driven two DQD battery, coherence also plays a dynamical role by accompanying and supporting population redistribution in the energy eigenbasis. Conversely, robust QB operation requires protecting not only the energy basis coherence, but also the population ordering pathway responsible for the dominant extractable work. The present analysis provides a basis for designing noise aware solid state QBs based on extractable work rather than injected energy alone. Natural extensions include the incorporation of relaxation processes, phonon assisted transitions, leakage outside the charge qubit subspace, and spatially correlated charge noise. Another important direction is the optimization of the tunnel coupling drive in order to identify operating regions where strong population ergotropy coexists with reduced detuning sensitivity. The same ergotropy channel decomposition can also be extended to larger

semiconductor QD arrays, where capacitive interactions and collective charge modes may offer additional routes toward robust and scalable QB charging.

ACKNOWLEDGMENTS

K. Loukhssami gratefully acknowledges financial support from CNRST Morocco through the PhD Associate Scholarship PASS initiative. The authors also acknowledge the National Center for Scientific and Technical Research (CNRST Morocco) for providing access to the HPC MARWAN computational infrastructure, which was used to perform the numerical simulations reported in this work.

Appendix A: Details of the numerical simulations

The numerical simulations presented in the main text are performed by averaging over stochastic realizations of the detuning charge noise. For each realization α , we generate independent noise traces $\delta\epsilon_i^{(\alpha)}(t)$ following the band limited $(1/f)$ power spectral density defined in Eq. (11). The dynamics is then obtained by solving the time-dependent Schrödinger equation

$$i\hbar \frac{d}{dt} |\psi_\alpha(t)\rangle = [H_B + H_{\text{ch}}(t) + H_n^{(\alpha)}(t)] |\psi_\alpha(t)\rangle, \quad (\text{A1})$$

where H_B is the static battery Hamiltonian, $H_{\text{ch}}(t)$ is the charging drive, and $H_n^{(\alpha)}(t)$ describes the stochastic detuning fluctuations. For each realization, we construct

$$\rho_\alpha(t) = |\psi_\alpha(t)\rangle\langle\psi_\alpha(t)|. \quad (\text{A2})$$

The noise-averaged state is then obtained as

$$\rho(t) = \frac{1}{N_r} \sum_{\alpha=1}^{N_r} \rho_\alpha(t). \quad (\text{A3})$$

In the final simulations, we use $N_r = 20000$ noise realizations. The Schrödinger equation is integrated using a fourth order Runge Kutta method. All observables, including the populations, coherence, ergotropy, its population and coherent contributions, and the passive ordering violation indicator $\mathcal{V}_{\text{pass}}$, are calculated from the averaged density matrix $\rho(t)$.

DATA AVAILABILITY

The numerical data and simulation scripts supporting the results of this study are available from the corresponding author upon reasonable request.

[1] A. E. Allahverdyan, R. Balian, and T. M. Nieuwenhuizen, *Europhysics Letters* **67**, 565 (2004).

[2] R. Alicki and M. Fannes, *Physical Review E* **87**, 042123 (2013).

- [3] K. V. Hovhannisyanyan, M. Perarnau-Llobet, M. Huber, and A. Ac'ın, *Physical Review Letters* **111**, 240401 (2013).
- [4] F. Campaioli, S. Gherardini, J. Q. Quach, M. Polini, and G. M. Andolina, *Reviews of Modern Physics* **96**, 031001 (2024).
- [5] G. Francica, F. C. Binder, G. Guarnieri, M. T. Mitchison, J. Goold, and F. Plastina, *Physical Review Letters* **125**, 180603 (2020).
- [6] F. Caravelli, B. Yan, L. P. García-Pintos, and A. Hama, *Quantum* **5**, 505 (2021).
- [7] H.-L. Shi, S. Ding, Q.-K. Wan, X.-H. Wang, and W.-L. Yang, *Physical Review Letters* **129**, 130602 (2022).
- [8] Z. Niu, Y. Wu, Y. Wang, X. Rong, and J. Du, *Physical Review Letters* **133**, 180401 (2024).
- [9] S. Tirone, R. Salvia, S. Chessa, and V. Giovannetti, *Physical Review A* **111**, 012204 (2025).
- [10] L. Li *et al.*, *Physical Review Research* **7**, 043236 (2025).
- [11] C.-J. Wang and F.-Q. Dou, *Chinese Physics Letters* **43**, 060602 (2026).
- [12] K. Loukhssami, K. El Hawary, H. Ait Mansour, and M. El Baz, *Physica Scripta* **101**, 135101 (2026).
- [13] F. A. Zwanenburg, A. S. Dzurak, A. Morello, M. Y. Simmons, L. C. L. Hollenberg, G. Klimeck, S. Rogge, S. N. Coppersmith, and M. A. Eriksson, *Reviews of Modern Physics* **85**, 961 (2013).
- [14] G. Burkard, T. D. Ladd, A. Pan, J. M. Nichol, and J. R. Petta, *Reviews of Modern Physics* **95**, 025003 (2023).
- [15] A. R. Mills, D. M. Zajac, M. J. Gullans, F. J. Schupp, T. M. Hazard, and J. R. Petta, *Nature Communications* **10**, 1063 (2019).
- [16] K. Petersson, J. R. Petta, H. Lu, and A. C. Gossard, *Physical Review Letters* **105**, 246804 (2010).
- [17] T. H. Oosterkamp, T. Fujisawa, W. G. van der Wiel, K. Ishibashi, R. V. Hijman, S. Tarucha, and L. P. Kouwenhoven, *Nature* **395**, 873 (1998).
- [18] T. Hayashi, T. Fujisawa, H.-D. Cheong, Y. H. Jeong, and Y. Hirayama, *Physical Review Letters* **91**, 226804 (2003).
- [19] K. E. Hawary, M. Azzouz, M. E. Baz, S. Deffner, B. Gardas, and Z. Mzaouali, *Physical Review E* **110**, 014120 (2024).
- [20] D. Kim, D. R. Ward, C. B. Simmons, J. K. Gamble, R. Blume-Kohout, E. Nielsen, D. E. Savage, M. G. Lagally, M. Friesen, S. N. Coppersmith, and M. A. Eriksson, *Nature Nanotechnology* **10**, 243 (2015).
- [21] S. N. Shevchenko, S. Ashhab, and F. Nori, *Physics Reports* **492**, 1 (2010).
- [22] X. Mi, S. Kohler, and J. R. Petta, *Physical Review B* **98**, 161404 (2018).
- [23] K. D. Petersson, C. G. Smith, D. Anderson, P. Atkinson, G. A. C. Jones, and D. A. Ritchie, *Physical Review Letters* **103**, 016805 (2009).
- [24] D. R. Ward, D. Kim, D. E. Savage, M. G. Lagally, R. H. Foote, M. Friesen, S. N. Coppersmith, and M. A. Eriksson, *npj Quantum Information* **2**, 16032 (2016).
- [25] E. R. MacQuarrie, S. F. Neyens, J. P. Dodson, J. Corrigan, B. Thorgrimsson, N. Holman, M. Palma, L. F. Edge, M. Friesen, S. N. Coppersmith, and M. A. Eriksson, *npj Quantum Information* **6**, 81 (2020).
- [26] H. A. Mansour, F. Siyouri, M. Faqir, and M. El Baz, *Physica Scripta* **95**, 095101 (2020).
- [27] S. Abaach, M. Faqir, and M. El Baz, *Physical Review A* **106**, 022421 (2022).
- [28] P. Dutta and P. M. Horn, *Reviews of Modern Physics* **53**, 497 (1981).
- [29] M. B. Weissman, *Reviews of Modern Physics* **60**, 537 (1988).
- [30] S. Kogan, *Electronic Noise and Fluctuations in Solids* (Cambridge University Press, 1996).
- [31] J. Schrieffer, Y. Makhlin, A. Shnirman, and G. Sch'on, *New Journal of Physics* **8**, 1 (2006).
- [32] E. Paladino, Y. M. Galperin, G. Falci, and B. L. Altshuler, *Reviews of Modern Physics* **86**, 361 (2014).
- [33] F. Beaudoin and W. A. Coish, *Physical Review B* **91**, 165432 (2015).
- [34] P. Sza'nkowski, G. Ramon, J. Krzywda, D. Kwiatkowski, and L. Cywi'nski, *Journal of Physics: Condensed Matter* **29**, 333001 (2017).
- [35] D. L. Mickelsen, H. M. Carruzzo, and C. C. Yu, *Physical Review B* **108**, 195307 (2023).
- [36] O. E. Dial, M. D. Shulman, S. P. Harvey, H. Bluhm, V. Umansky, and A. Yacoby, *Physical Review Letters* **110**, 146804 (2013).
- [37] B. M. Freeman, J. S. Schoenfield, and H. Jiang, *Applied Physics Letters* **108**, 253108 (2016).
- [38] L. Petit, J. M. Boter, H. G. J. Eenink, G. Droulers, M. L. V. Tagliaferri, R. Li, D. P. Franke, K. J. Singh, J. S. Clarke, R. N. Schouten, V. V. Dobrovitski, L. M. K. Vandersypen, and M. Veldhorst, *Physical Review Letters* **121**, 076801 (2018).
- [39] E. J. Connors, J. Nelson, H. Qiao, L. F. Edge, and J. M. Nichol, *Physical Review B* **100**, 165305 (2019).
- [40] E. J. Connors, J. Nelson, L. F. Edge, and J. M. Nichol, *Nature Communications* **13**, 940 (2022).
- [41] J. A. Krzywda and Ł. Cywi'nski, *Physical Review B* **101**, 035303 (2020).
- [42] P. Huang, N. M. Zimmerman, and G. W. Bryant, *npj Quantum Information* **4**, 62 (2018).
- [43] Y.-C. Yang, S. N. Coppersmith, and M. Friesen, *Physical Review A* **100**, 022337 (2019).
- [44] F. Motzoi, J. M. Gambetta, P. Rebentrost, and F. K. Wilhelm, *Physical Review Letters* **103**, 110501 (2009).
- [45] F. Motzoi and F. K. Wilhelm, *Physical Review A* **88**, 062318 (2013).
- [46] H.-O. Li, G. Cao, G.-D. Yu, M. Xiao, G.-C. Guo, H.-W. Jiang, and G.-P. Guo, *Nature communications* **6**, 7681 (2015).
- [47] B. Thorgrimsson, D. Kim, Y.-C. Yang, L. Smith, C. Simmons, D. R. Ward, R. H. Foote, J. Corrigan, D. Savage, M. Lagally, *et al.*, *npj Quantum Information* **3**, 32 (2017).
- [48] F. Binder, S. Vinjanampathy, K. Modi, and J. Goold, *Physical Review E* **91**, 032119 (2015).
- [49] F. Campaioli, F. A. Pollock, F. C. Binder, L. Céleri, J. Goold, S. Vinjanampathy, and K. Modi, *Physical review letters* **118**, 150601 (2017).
- [50] W. Pusz and S. L. Woronowicz, *Communications in Mathematical Physics* **58**, 273 (1978).
- [51] A. Lenard, *Journal of Statistical Physics* **19**, 575 (1978).
- [52] E. Chitambar and G. Gour, *Physical Review A* **94**, 052336 (2016).
- [53] T. Baumgratz, M. Cramer, and M. B. Plenio, *Physical Review Letters* **113**, 140401 (2014).
- [54] A. Streltsov, G. Adesso, and M. B. Plenio, *Reviews of Modern Physics* **89**, 041003 (2017).
- [55] A. P. Majtey, P. W. Lambert, and D. P. Prato, *Physical Review A* **72**, 052310 (2005).
- [56] P. W. Lambert, A. P. Majtey, A. Borrás, M. Casas, and A. Plastino, *Physical Review A* **77**, 052311 (2008).

- [57] C. Radhakrishnan, M. Parthasarathy, S. Jambulingam, and T. Byrnes, [Physical Review Letters](#) **116**, 150504 (2016).
- [58] B. Paquelet Wuetz, D. Degli Esposti, A.-M. J. Zwerver, S. V. Amitonov, M. Botifoll, J. Arbiol, A. Sammak, L. M. K. Vandersypen, M. Russ, and G. Scappucci, [Nature Communications](#) **14**, 1385 (2023).